geoconvention
Calgary • Canada • May 15-19 2017

Quantifying parameter trade-off in elastic full-waveform inversion via multi-parameter Hessian probing

Wenyong Pan[1], Kris Innanen[1], Yanhua Yuan[2], Frederik Simons[2]

1 Department of Geoscience, CREWES Project, University of Calgary

2 Department of Geoscience, Princeton University

Summary

Inverting multiple physical parameters in subsurface using full-waveform inversion (FWI) methods suffer from interparameter tradeoffs arising from inherent ambiguities between different physical parameters. In recent years, people have devoted intensive efforts for evaluating the resolving abilities of different parameterizations in elastic and anisotropic FWI based on analytic solutions of the Fréchect derivative wavefields. However, we find that the scattering patterns may do not provide enough information about the interparameter contaminations. In this research, we propose to evaluate the interparameter coupling effects via probing multiparameter Hessian, which provides more complete and direct measurements of the interparameter contaminations.

Introduction

In recent decades, full-waveform inversion (FWI) methods become increasing popular in global- and exploration-scale geophysics for the capabilities of providing high-resolution estimates of subsurface properties (Tarantola, 1984; Pratt et al.,1998; Pan et al., 2014a). Elastic and anisotropic parameters are essentially important for reservoir characterization (Yuan et al., 15). Simultaneously reconstructing multiple physical parameters suffers from parameter crosstalk problem arising from the inherent ambiguities among these parameters (Tarantola, 1986; Innanen, 2014). This research aims at quantifying the interparameter contaminations of isotropic-elastic parameters and understanding how do they affect the inversion process.

For mitigating the parameter crosstalk difficulty in multiparameter FWI, researchers have devoted intensive efforts on the parameter resolution studies based on analytic solutions of Frechéct derivative wavefields for different parameter classes (Tarantola, 1986; Pan et al., 2016). Coupling effects appear between two different physical parameters, if the scattered wavefileds due to the model perturbations overlap at certain range of scattering angle. However, we find that the scattering patterns may do not provide complete information about the interparameter tradeoffs due to a series of assumptions. These assumptions may result in the following defects: (1) complex physics background and geological structures are not considered; (2) finite-frequency effects and travel time contribution are ignored; (3) the spatial correlations of different physical parameters are not considered; (4) influences of multicomponents data are not evaluated.

Hessian operator represents the second derivative of the misfit function, describes the geometry of the objective function in terms of curvature or convexity, and provides complete and direct measurements of spatial and interparameter tradeoffs (Kuo and Romanowicz, 2002; Fichtner and van Leeuwen, 2015). Elements in off-diagonal blocks measure the correlations of different physical parameters (Pan et al., 2015; Pan et al., 2016; Pan et al., 2017). For large-scale inverse problems, it is unaffordable to construct multiparameter Hessian explicitly. In this paper, we will show that how to quantify the interparameter contaminations via probing multiparameter Hessian.

Multiparameter Isotropic-elastic Full-waveform Inversion

Full-waveform inversion (FWI) seeks to estimate the subsurface (an) elastic and anisotropic properties by iteratively minimizing the differences between seismic observations and synthetic data. The misfit function is formulated as L-2 norm (Pratt et al., 1998; Yuan et al., 14; Pan et al., 2014b):

$$\Phi(\mathrm{m}) = \frac{1}{2}\sum_{s=1}^{S}\sum_{r=1}^{R}\left\|\Delta \mathrm{d}(x_s, x_r, t; \mathrm{m})\right\| dt, \tag{1}$$

where $\Delta \mathrm{d}(x_s, x_r, t; \mathrm{m})$ is the data residual. In order to solve the inverse problem, the model is always updated iteratively. Within the Newton optimization framework, the search direction can be obtained by solving the Newton linear system: $\mathrm{H}_k \Delta \mathrm{m}_k = -\nabla_m \Phi_k$, where $\nabla_m \Phi_k$ and H_k are gradient and Hessian respectively. Gradient of the misfit function corresponding to Bulk modulus κ, shear modulus μ and density ρ can be expressed as:

$$\begin{aligned}\nabla_m \Phi(\mathrm{m}) = -\sum_{s=1}^{S}\sum_{r=1}^{R}\int_0^T\int_{\Omega(\mathrm{x})}\int_0^t \Big[\Delta\rho(\mathrm{x})G_{ni}(\mathrm{x},\mathrm{x}_r,t-t')\partial_t^2 u_i(\mathrm{x},\mathrm{x}_s,t') + \left(\Delta\kappa(\mathrm{x}) - \frac{2}{3}\Delta\mu(\mathrm{x})\right)\delta_{ij}\delta_{kl}\delta_j G_{ni}(\mathrm{x},\mathrm{x}_r,t-t')\partial_k u_l(\mathrm{x},\mathrm{x}_s,t') \\ + \Delta\mu(\mathrm{x})\left(\delta_{ik}\delta_{jl}+\delta_{jk}\delta_{il}\right)\delta_j G_{ni}(\mathrm{x},\mathrm{x}_r,t-t')\partial_k u_l(\mathrm{x},\mathrm{x}_s,t')\Big]\Delta \mathrm{d}(x_s,x_r,t;\mathrm{m})\,dt'd\mathrm{x}dt,\end{aligned} \tag{3}$$

where G_{ni} is the Green's function. Explicit expressions of the sensitivity kernels for bulk modulus κ, shear modulus μ and density ρ are given by:

$$\begin{aligned}K_\kappa &= -\sum_{s=1}^{S}\sum_{r=1}^{R}\int_0^T\int_{\Omega(\mathrm{x})}\kappa(\mathrm{x})\left[\nabla\cdot \mathrm{u}^*(\mathrm{x}_r,\mathrm{x},T\text{-}t)\right]\left[\nabla\cdot \mathrm{u}(\mathrm{x},\mathrm{x}_s,t)\right]dtd\mathrm{x}, \quad K_\mu = -\sum_{s=1}^{S}\sum_{r=1}^{R}\int_0^T\int_{\Omega(\mathrm{x})} 2\mu(\mathrm{x})\mathrm{D}^*(\mathrm{x}_r,\mathrm{x},T\text{-}t):\mathrm{D}(\mathrm{x},\mathrm{x}_s,t)dtd\mathrm{x}, \\ K_\rho &= -\sum_{s=1}^{S}\sum_{r=1}^{R}\int_0^T\int_{\Omega(\mathrm{x})}\rho(\mathrm{x})\mathrm{u}^*(\mathrm{x}_r,\mathrm{x},T\text{-}t)\partial_t^2\mathrm{u}(\mathrm{x},\mathrm{x}_s,t)dtd\mathrm{x},\end{aligned} \tag{4}$$

where D is the traceless strain deviator. The sensitivity kernels for P-wave velocity α, shear-wave velocity β and density ρ' are given by:

$$K_\alpha = 2\left(1+\frac{4\mu}{3\kappa}\right)K_\kappa, K_\beta = 2\left(K_\mu - \frac{4\mu}{3\kappa}\right)K_\kappa, K_{\rho'} = K_\kappa + K_\mu + K_\rho. \tag{5}$$

For understanding the origin of the interparameter tradeoffs, the Newton linear system can be written as:

$$\nabla_\alpha \Phi = K_{\alpha\leftrightarrow\alpha} + K_{\beta\to\alpha} + K_{\rho'\to\alpha} = -\int_{\Omega(\mathrm{x})}\int_{\Omega(\mathrm{x}')} H_{\alpha\alpha}(\mathrm{x},\mathrm{x}')\Delta m_\alpha(\mathrm{x}')d\mathrm{x}'d\mathrm{x} - \int_{\Omega(\mathrm{x})}\int_{\Omega(\mathrm{x}')} H_{\alpha\beta}(\mathrm{x},\mathrm{x}')\Delta m_\beta(\mathrm{x}')d\mathrm{x}'d\mathrm{x} - \int_{\Omega(\mathrm{x})}\int_{\Omega(\mathrm{x}')} H_{\alpha\rho'}(\mathrm{x},\mathrm{x}')\Delta m_{\rho'}(\mathrm{x}')d\mathrm{x}'d\mathrm{x}, \tag{6}$$

where $K_{\alpha\leftrightarrow\alpha}$ represents the correct update for α, $K_{\beta\to\alpha}$ and $K_{\rho'\to\alpha}$ are interparameter tradeoff kernels indicating contaminations from β and ρ' to α, which are described by multiparameter Hessian diagonal blocks $\mathrm{H}_{\alpha\beta}$ and $\mathrm{H}_{\alpha\rho'}$. Similarly, the contaminations from α and ρ' to β are obtained as:

$$K_{\alpha\to\beta} = -\int_{\Omega(\mathrm{x})}\int_{\Omega(\mathrm{x}')} H_{\beta\alpha}(\mathrm{x},\mathrm{x}')\Delta m_\alpha(\mathrm{x}')d\mathrm{x}'d\mathrm{x}, K_{\rho'\to\beta} = -\int_{\Omega(\mathrm{x})}\int_{\Omega(\mathrm{x}')} H_{\beta\rho'}(\mathrm{x},\mathrm{x}')\Delta m_{\rho'}(\mathrm{x}')d\mathrm{x}'d\mathrm{x}. \tag{7}$$

And the contaminations from α and β to ρ' are given by:

$$K_{\alpha\to\rho'} = -\int_{\Omega(\mathrm{x})}\int_{\Omega(\mathrm{x}')} H_{\rho'\alpha}(\mathrm{x},\mathrm{x}')\Delta m_\alpha(\mathrm{x}')d\mathrm{x}'d\mathrm{x}, K_{\beta\to\rho'} = -\int_{\Omega(\mathrm{x})}\int_{\Omega(\mathrm{x}')} H_{\rho'\beta}(\mathrm{x},\mathrm{x}')\Delta m_\beta(\mathrm{x}')d\mathrm{x}'d\mathrm{x}. \tag{8}$$

Gradient updates are linear combinations of correct model estimations with parameter crosstalk artifacts which are determined by both of model perturbations and multiparameter Hessian off-diagonal blocks.

Multiparameter Hessian Probing

Off-diagonal blocks of multiparameter Hessian provide direct measurements of parameter leakages in a generalized inversion framework. However, it is unaffordable to construct the whole matrix explicitly, when the number of model parameters to be inverted is very large. Matrix probing techniques can be employed to extract partial information from Hessian or infer the characteristics of Hessian. Considering

the perturbations of S-wave velocity and density are zeros and P-wave velocity perturbation is point localized at position $\tilde{\mathrm{x}}$: $\Delta \mathrm{m}_{\alpha}(\tilde{\mathrm{x}}) = A_{\alpha}\delta(\mathrm{x}-\tilde{\mathrm{x}})$, the Newton system becomes:

$$\nabla_{\alpha}\Phi = K_{\alpha\leftrightarrow\alpha} = -A_{\alpha}\int_{\Omega(\mathrm{x})}\int_{\Omega(\mathrm{x}')} H_{\alpha\alpha}(\mathrm{x},\mathrm{x}')\delta(\mathrm{x}'-\tilde{\mathrm{x}})d\mathrm{x}'d\mathrm{x} = -A_{\alpha}\mathrm{H}_{\alpha\alpha}(\tilde{\mathrm{x}}), K_{\alpha\to\beta} = -A_{\alpha}\mathrm{H}_{\beta\alpha}(\tilde{\mathrm{x}}), K_{\alpha\to\rho'} = -A_{\alpha}\mathrm{H}_{\rho'\alpha}(\tilde{\mathrm{x}}), \tag{9}$$

where $\mathrm{H}_{\alpha\alpha}(\tilde{\mathrm{x}})$, $\mathrm{H}_{\beta\alpha}(\tilde{\mathrm{x}})$ and $\mathrm{H}_{\rho'\alpha}(\tilde{\mathrm{x}})$ form one multiparameter Hessian column named as multiparameter point spread functions (MPSFs), which allow us to quantify the spatial correlations of different physical parameters locally by taking finite-frequency effects into consideration. If constant perturbation of P-wave velocity is applied in the whole volume, we are able to calculate the MPSFs volumes.

Numerical Examples

In this section, we examine the interparameter contaminations with numerical examples. Figure 1 show the multiparameter point spread functions (MPSFs) with multicomponent and single component data respectively. We observe that positive P-wave velocity perturbation produce negative and positive contaminations in S-wave velocity and density respectively. S-wave velocity produce strong contaminations in P-wave velocity and density. With x-component, the contaminations due to S-wave velocity appear to be stronger than those of z-component data.

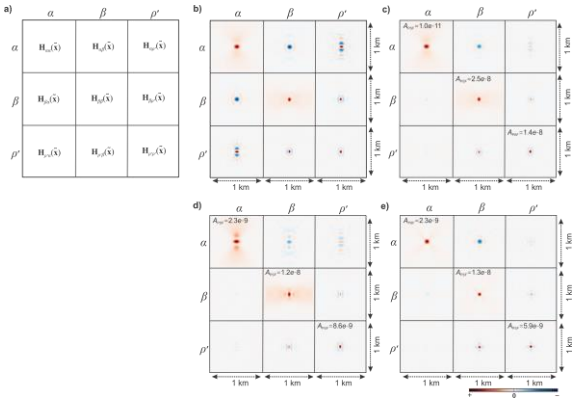

Figure 1. (a) show the multiparameter point spread functions (MPSFs) arranged as the structure of multiparameter Hessian; (b) and (c) show the MPSFs before and after normalization with x-z component data; (d) and (e) show the corresponding MPSFs with z-and x-component data respectively.

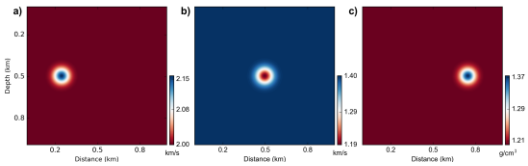

Figure 2. (a), (b) and (c) show the true P-wave velocity, S-wave velocity and density models with 3 isolated Gaussian anomalies.

To verify our predictions, we carry out inversion experiments. Figure 2 show the true models with 3 isolated Gaussian anomalies. The initial models are homogeneous. Sources and receivers are arranged along on all boundaries of the model. Figure 3 show the sensitivity kernels with multicomponent data and single component data respectively in the first iteration. As we can see, contaminations from S-wave velocity to P-wave velocity and density are very strong, especially when using x-component data. Figure 4 show the inverted models after 10 iterations. P-wave velocity suffers contaminations from S-wave velocity and density and is poorest inverted. S-wave velocity is best inverted especially when using x-component data. Inverted density model is also contaminated by parameter crosstalk artifacts. We then examine the interparameter contaminations using a more complex Marmousi model. Figure 5 show the true models, initial models and true model perturbations respectively. Panel 6a show the sensitivity kernels calculated using the models shown in Figure 5. To evaluate the interparameter contaminations, we calculate the correct updates $K_{\alpha\leftrightarrow\alpha}$, $K_{\beta\leftrightarrow\beta}$ and $K_{\rho'\leftrightarrow\rho'}$ and the interparameter contamination kernels. As

we can see, S-wave velocity suffers from limited contaminations. The influences of interparameter contaminations to P-wave velocity are also not obvious. Density suffers from strong contaminations mainly from S-wave velocity.

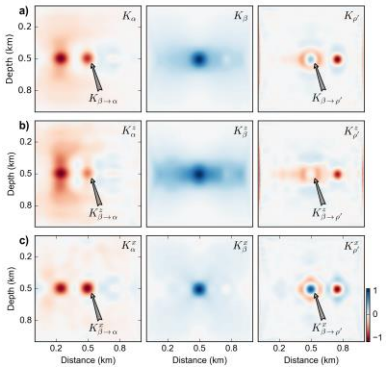

Figure 3. (a) illustrate the sensitivity kernels for P-wave velocity, S-wave velocity and density with x-z component data; (b) and (c) show the z- and x-component sensitivity kernels respectively.

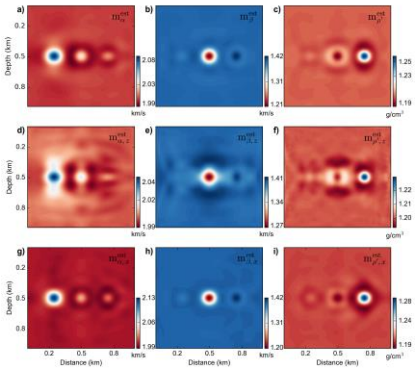

Figure 4. Panels (a-c) show the inverted P-wave velocity, S-wave velocity and density models using x-z component data; (d-f) and (g-i) are inverted models using z- and x-component data respectively.

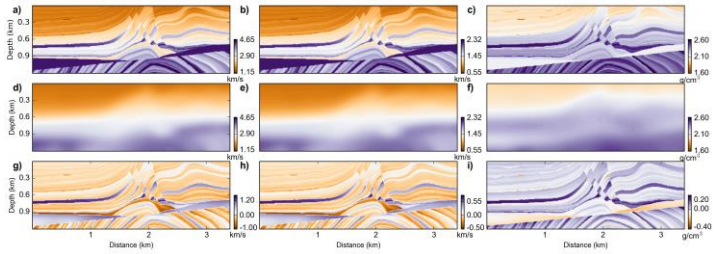

Figure 5. (a), (b) and (c) show the true P-wave velocity, S-wave velocity and density models; (d), (e) and (f) show the corresponding initial models; (g), (h) and (i) are the true model perturbations of these parameters.

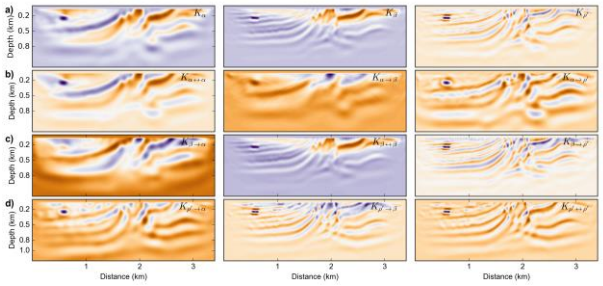

Figure 6. Panel (a) shows the sensitivity kernels K_α , K_β and $K_{\rho'}$; Panel (b) show the correct update $K_{\alpha\leftrightarrow\alpha}$, contamination kernels $K_{\alpha\to\beta}$ and $K_{\alpha\to\rho'}$; Panel (c) show the correct update $K_{\beta\leftrightarrow\beta}$, contamination kernels $K_{\beta\to\alpha}$ and $K_{\beta\to\rho'}$; Panel (d) show the correct update $K_{\rho'\leftrightarrow\rho'}$, contamination kernels $K_{\rho'\to\alpha}$ and $K_{\rho'\to\beta}$.

Conclusions

In this paper, we evaluate the interparameter contaminations between different physical parameters in isotropic-elastic FWI with multiparameter Hessian probing. It is observed that S-wave velocity suffers from limited parameter crosstalk artifacts. However, density is contaminated by strong artifacts due to S-wave velocity perturbation.

Acknowledgements

This research was supported by the Consortium for Research in Elastic Wave Exploration Seismology (CREWES) and National Science and Engineering Research Council of Canada (NSERC, CRDPJ 461179-13). Wenyong Pan is also supported by SEG/Chevron scholarship and Eyes High International Doctoral Scholarship.

References

Pratt, R. G., C. Shin, and G. J. Hicks, 1998, Gauss-Newton and full Newton methods in frequency-space seismic waveform inversion: Geophysical Journal International, 133, 341-362.

Pan, W., K. A. Innanen, and G. F. Margrave, 2014a, A comparison of different scaling methods for least-squares migration/inversion: EAGE Expanded Abstracts, We G103 14.

Pan, W., G. F. Margrave, and K. A. Innanen, 2014b, Iterative modeling migration and inversion (IMMI): Combining full waveform inversion with standard inversion methodology: SEG Technical Program Expanded Abstracts, 938-943.

Pan, W., K. A. Innanen, G. F. Margrave, and D. Cao, 2015, Efficient pseudo-Gauss-Newton full-waveform inversion in the t-p domain: Geophysics, 80, no. 5, R225-R14.

Pan, W., K. A. Innanen, G. F. Margrave, M. C. Fehler, X. Fang, and J. Li, 2016, Estimation of elastic constants for HTI media using Gauss-Newton and full-Newton multiparameter full-waveform inversion: Geophysics, 81 (5), R275-R291.

Pan, W., K. A. Innanen, and W. Liao, 2017, Accelerating Hessian-free Gauss-Newton full-waveform inversion via *l*-BFGS preconditioned conjugate-gradient algorithm: Geophysics, 82 (2), 1-16.

Tarantola, A., 1984, Inversion of seismic reflection data in the acoustic approximation: Geophysics, 49, 1259-1266.

Tarantola, A., 1986, A strategy for nonlinear elastic inversion of seismic reflection data: Geophysics, 51, 1893–1903

Virieux, A. and S. Operto, 2009, An overview of full-waveform inversion in exploration geophysics: Geophysics, 74, no. 6, WCC1-WCC26.

Innanen, K. A., 2014, Seismic AVO and the inverse Hessian in precritical reflection full waveform inversion: Geophysical Journal International,199, 717–734.

Yanhua, Y. O. and F. J. Simons, 2014, Multiscale adjoint waveform difference tomography using wavelets: Geophysics, 79, no. 3, WA79–WA95.

Yanhua, Y. O., F. J. Simons, and E. Bozdaˇg, 2015, Multiscale adjoint waveform tomography for surface and body waves: Geophysics, 80, no. 5, R281–R302.